Journal of the Optical Society of America B
OPTICAL PHYSICS

Hyperpolarizability dispersion measured for CS_2 vapor

RODRIGO N. FERNANDEZ AND DAVID P. SHELTON*

Department of Physics and Astronomy, University of Nevada, Las Vegas, Nevada 89154-4002, USA
**Corresponding author: shelton@physics.unlv.edu*

Received 2 April 2020; revised 21 April 2020; accepted 26 April 2020; posted 27 April 2020 (Doc. ID 394315); published 20 May 2020

The second hyperpolarizability (γ) of carbon disulfide (CS_2) is measured by gas-phase electric-field-induced second-harmonic generation for laser wavelengths in the range 765–1064 nm. The observed hyperpolarizability is decomposed into electronic (γ^e) and vibrational (γ^v) contributions, and the dispersion curve for γ^e is extrapolated to the static limit, with the result of $\gamma_0^e = 12558 \pm 93$ atomic units $= 7.83 \pm 0.06 \times 10^{-61}$ C^{4}m^{4}J^{-3} $= 6.33 \pm 0.05 \times 10^{-36}$ esu (Taylor series convention). The results of this experiment agree with other recent nonlinear optical measurements and theoretical calculations.

https://doi.org/10.1364/JOSAB.394315

1. INTRODUCTION

Carbon disulfide is a molecule that has been extensively studied, is widely used for its nonlinear optical (NLO) properties, and is literally the textbook example for many NLO processes [1]. Liquid CS_2 is often used in applications, or as a reference standard for NLO measurements, due to its transparency and large nonlinear refractive index. It has a strong response on the ps time scale due to molecular reorientation, libration, and translation, and a smaller response on the fs time scale due to electronic and vibrational contributions [2–6]. However, the complicated time, frequency, and polarization-dependent response for CS_2 makes its use as a reference problematic [2,6], which has motivated investigations of the individual contributions to better understand the combined NLO response for CS_2.

The fast, fs NLO response for CS_2 is governed by the electronic and vibrational contributions to the molecular hyperpolarizability, $\gamma = \gamma^e + \gamma^v$. The first measurements of the molecular hyperpolarizability for CS_2 used the DC Kerr effect in the gas phase [7] and electric-field-induced second-harmonic generation (ESHG) in the liquid phase [8]. Following these experiments, there has been a succession of theoretical calculations of increasing sophistication for γ of CS_2 [9–12], none of which agrees with the early experimental results. Only recently have there been further experiments making absolute measurements of γ in the gas phase [13,14] and liquid phase [2,3] for CS_2. The results of these recent experiments contradict the earlier experimental results and are close to the theoretical calculations.

The experimental study in this work presents measurements of γ for CS_2 made with high accuracy using the technique of gas-phase ESHG with periodic phase matching [15–18], over a range of wavelengths to produce a dispersion curve. The experiment is described first and the results are presented. Then, the experimental dispersion curve is combined with the results of recent theoretical calculations to decompose the hyperpolarizability into electronic and vibrational contributions. Finally, the results of the present experiment are compared to the other experimental measurements and the theoretical calculations.

2. EXPERIMENT

The ESHG experimental method is similar to that previously described [15,17]. Second-harmonic light is generated by the laser beam in a gas sample when a transverse static electric field is applied to the gas. In this experiment, a spatially alternating static electric field is applied to the gas by a periodic array of N electrode pairs, and the ESHG signal is increased by a factor of N^2 when the coherence length in the gas is adjusted to match the longitudinal period of the electrode array. The gas density ρ controls the coherence length, and ρ is scanned to find the phase-matching density and maximum second-harmonic signal $S^{(2\omega)}$. The ratio of hyperpolarizabilities γ for two gases is determined from measurements of the peak signal $S^{(2\omega)}$ and gas density ρ at phase-match for each of the gases, where CS_2 and N_2 are the sample and reference gases in the present experiment. The hyperpolarizability ratio is given by [17]

$$\frac{\gamma_{CS_2}}{\gamma_{N_2}} = \left[\frac{S^{(2\omega)}_{CS_2}}{S^{(2\omega)}_{N_2}}\right]^{1/2} \left[\frac{\rho_{CS_2} n'_{CS_2} V_{CS_2}}{\rho_{N_2} n'_{N_2} V_{N_2}}\right]^{-1}, \tag{1}$$

where

$$n' = (n_0^4 n_\omega^3 n_{2\omega})^{1/6}, \tag{2}$$

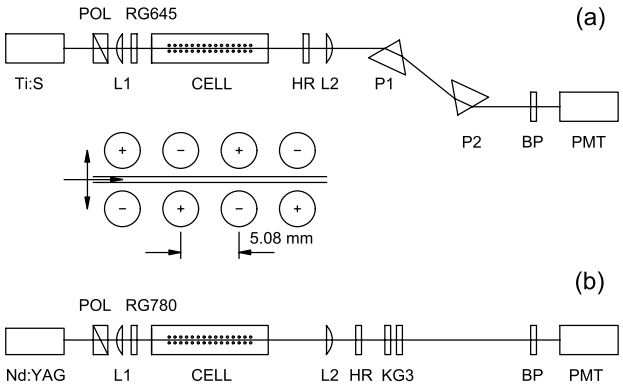

Fig. 1. Schematic diagram of the experimental apparatus described in the text, using (a) a cw Ti:sapphire laser for wavelengths 765–900 nm, or (b) a pulsed Nd:YAG laser at 1064 nm. The inset shows the path of the focused linear polarized laser beam between cylindrical electrodes with alternating polarity in the gas cell.

n_ω is the gas refractive index at frequency ω, and V is the electrode array voltage.

Figure 1 shows schematic diagrams of the experimental apparatus. A cw Ti:sapphire laser (folded linear resonator with 0.5–0.9 W output power and <1 GHz bandwidth) was used for measurements in the 765–900 nm wavelength range, and a pulsed Nd:YAG (yttrium aluminum garnet) laser (0.4 mJ, 100 ns pulses, 4 kHz repetition rate, 20 GHz bandwidth) was used for measurements at 1064 nm. The Ti:sapphire laser frequency was measured with a scanning Michelson wavemeter (Burleigh WA-20).

A laser beam with the desired linear polarization state (optical field polarized parallel to the static electric field) is prepared by the prism polarizer (POL), lens L1 focuses the beam to 20 cm confocal parameter with a waist at the center of the gas cell (CELL), and a red glass filter (Schott RG645 or RG780) blocks any light at the second-harmonic wavelength that may be present in the incident beam before it enters the gas cell. ESHG occurs as the laser beam passes between the electrodes in the gas cell (Fig. 1 inset). The transmitted fundamental beam and coaxial second-harmonic beam generated in the gas cell are collimated by lens L2 and separated by a sequence of spectral filters. The filters for the cw laser experiment [Fig. 1(a)] are a laser mirror (HR) with high reflectivity for the fundamental and high transmission for the second harmonic, a tandem Brewster prism spectrometer (P1, P2), and a band pass interference filter for the second-harmonic light (BP). The filters for the pulsed laser experiment [Fig. 1(b)] are similar, except that the prism spectrometer is replaced by several infrared absorbing glass filters (Schott KG3). The second-harmonic beam is detected by a photon-counting photomultiplier tube (PMT).

The coherence length for SHG, $l_c = \pi/|2k_\omega - k_{2\omega}|$ where $k_\omega = 2\pi n_\omega/\lambda_\omega$, is determined by the refractive index dispersion. The coherence length for SHG in a gas is proportional to $\lambda^3\rho^{-1}$ [19], so an electrode array with a shorter period requires a higher gas density to reach phase match, but it generates a larger ESHG signal. In these experiments, the period of the electrode array is constrained by the 360 Torr vapor pressure for CS_2 at room temperature. The array for the cw laser measurements has 82 pairs of cylindrical electrodes with 3.18 mm diameter and 5.08 mm spacing (Fig. 1 inset), and phase match for the 765–900 nm laser wavelength range occurs at 100–300 Torr CS_2 gas pressure. The maximum applied field was limited to avoid breakdown in the gas, so the array voltage increased from 1 to 3 kV and the ESHG photon count signal increased from 10 to 30 s^{-1} over this wavelength range for CS_2. The breakdown voltage and ESHG signal were larger for the N_2 reference gas. For a typical N_2 measurement, the phase match pressure, array voltage, and ESHG signal were 4000 Torr, 5 kV and 200 s^{-1}.

The first measurements for CS_2 were made at 1064 nm with the pulsed laser, and since the dispersion was uncertain, an array with a very long period was constructed to ensure that phase match would be possible. The array for the pulsed laser measurement also had 82 pairs of cylindrical electrodes with 3.18 mm diameter and 5.08 mm spacing, but they were electrically connected in groups of six to increase the period. The 1064 nm measurements were made at 251 Torr for CS_2, using the phase-match peak at three times the density of the lowest-density phase-match peak [15]. The pulsed laser ESHG signal with 1 kV array voltage was about 1000 s^{-1} for both CS_2 and N_2. The usual correction was made for photon counting dead time {Eq. (7) in Ref. [17]}.

Alternating measurements (ABABA…) were made for the sample and reference gas to cancel the effect of slow signal drift during the measurements. Hyperpolarizability ratios were determined from triplets of measurements: each signal ratio was the sample signal divided by the average of the reference signals immediately before and after that sample signal measurement. The small incoherent background was measured and subtracted. Coherent background was assessed by reversing the array polarity [17] and found to be negligible (<0.1% of signal). The sample and reference beam paths are slightly different due to the different refractive indices for the sample and reference gas filling the cell. The beam is carefully centered in the array and aligned through the following optics to prevent a systematic error in the measured signal ratio due to the small change in the beam path.

Gas densities appearing in Eq. (1) were determined with <0.1% uncertainty from the measured gas pressure and temperature at phase match using the virial equation of state [20]. The sample gas temperature was 295 ± 1K. The gas refractive index was determined using the measured gas density and published refractive index data [21]. The largest contribution to the hyperpolarizability ratio uncertainty was due to photon-counting statistics, with statistical uncertainty 0.4–1.5% for a single triplet of measurements and 3–12 triplets contributing to the final results.

3. RESULTS AND DISCUSSION

The hyperpolarizability ratios $\gamma_{CS_2}/\gamma_{N_2}$ and phase-match density ratios ρ_{N_2}/ρ_{CS_2} measured in this experiment are given in Table 1. The results for γ_{CS_2} are also given in Table 1, and are obtained from $\gamma_{CS_2}/\gamma_{N_2}$ using the previously determined ESHG dispersion curve for γ_{N_2} [17]:

$$\gamma_{N_2} = \gamma^e_{0,N_2}(1 + Av_L^2 + Bv_L^4) + Gv^{-2} + Hv^{-4}, \quad (3)$$

Table 1. ESHG Phase-Match Density Ratio and Hyperpolarizability Ratio Measurements for CS_2 and N_2, and Experimental Results for γ_{CS_2} in Atomic Units

λ (nm)	$\nu(\mathrm{cm}^{-1})$	ρ_{N_2}/ρ_{CS_2}	$\gamma_{CS_2}/\gamma_{N_2}$	$\gamma_{CS_2}(10^3\,\mathrm{au})$
1064	9395	19.50 ± 0.02	15.59 ± 0.02	15.07 ± 0.04
900	11111.1	20.24 ± 0.02	16.46 ± 0.06	16.33 ± 0.07
880	11363.4	20.39 ± 0.02	16.65 ± 0.06	16.58 ± 0.07
860	11627.9	20.66 ± 0.02	16.71 ± 0.08	16.71 ± 0.09
840	11904.8	20.78 ± 0.02	17.00 ± 0.08	17.09 ± 0.09
820	12195.3	21.00 ± 0.02	17.24 ± 0.08	17.43 ± 0.09
810	12345.1	21.13 ± 0.02	17.27 ± 0.09	17.50 ± 0.09
800	12500.0	21.26 ± 0.02	17.41 ± 0.04	17.69 ± 0.05
790	12658.1	21.41 ± 0.02	17.39 ± 0.06	17.73 ± 0.07
780	12820.5	21.51 ± 0.02	17.43 ± 0.07	17.82 ± 0.08
765	13071.9	21.73 ± 0.02	17.73 ± 0.09	18.21 ± 0.10

where $\nu_L^2 = 6\nu^2$ for ESHG. Expressing γ in atomic units ($1\,\mathrm{au} = 6.235377 \times 10^{-65}\ \mathrm{C^4m^4J^{-3}}$) and ν in cm^{-1}, the coefficients in Eq. (3) are $\gamma^e_{0,N_2} = 917.35$ au, $A = 1.003 \times 10^{-10}\ \mathrm{cm}^2$, $B = 1.852 \times 10^{-20}\ \mathrm{cm}^4$, $G = -3.544 \times 10^8$ au cm^{-2}, and $H = -1.668 \times 10^{15}$ au cm^{-4}. The uncertainty for γ_{CS_2} includes an estimated uncertainty of 0.2% for the γ_{N_2} reference.

The form of Eq. (3) for γ_{N_2} is an example of a more general result, where the electronic contribution to $\gamma(-\nu_\sigma; \nu_1, \nu_2, \nu_3)$ at frequencies far below the electronic resonance frequencies is an even power series in ν_L [22,23], where $\nu_\sigma = \nu_1 + \nu_2 + \nu_3$ and

$$\nu_L^2 = \nu_\sigma^2 + \nu_1^2 + \nu_2^2 + \nu_3^2. \tag{4}$$

There is also a pure vibrational contribution to γ with resonances at vibration transition frequencies. For frequencies far above vibrational resonance, this contribution is given by the sum of terms in even inverse powers of ν. Vibrational resonances distinguish this contribution from the effect of zero-point vibration averaging (ZPVA), which is included in the experimental electronic contribution. The polarizability α and hyperpolarizability γ of CS_2 far-off resonance will have a form similar to Eq. (3).

Figure 2(a) shows the data for ρ_{N_2}/ρ_{CS_2} plotted versus ν_L^2. The inverse phase-match density ρ^{-1} is proportional to the polarizability dispersion $\Delta\alpha(\nu) = \alpha(2\nu) - \alpha(\nu)$, so $\rho_{N_2}/\rho_{CS_2} = \Delta\alpha_{CS_2}/\Delta\alpha_{N_2}$ measures the polarizability dispersion for CS_2. The function fit to the data is constructed from $\alpha(\nu)$ for CS_2 and N_2. The electronic polarizability $\alpha^e(\nu)$ below resonance is a power series in ν^2, and the expression for the electronic contribution to $\Delta\alpha$ has the form

$$\Delta\alpha^e = c_1\nu^2(1 + c_2\nu^2 + c_3\nu^4). \tag{5}$$

For N_2, there is no pure vibrational contribution to α, so $\Delta\alpha_{N_2} = \Delta\alpha^e_{N_2}$. The coefficients in Eq. (5) for $\Delta\alpha^e_{N_2}$ determined from previous experimental measurements [19,24] are $c_{1,N_2} = 1.8905 \times 10^{-9}\ \mathrm{au\,cm}^2$, $c_{2,N_2} = 3.076 \times 10^{-10}\ \mathrm{cm}^2$, and $c_{3,N_2} = 17.58 \times 10^{-20}\ \mathrm{cm}^4$, where ν is in cm^{-1} and α is in atomic units ($1\,\mathrm{au} = 1.648778 \times 10^{-41}\ \mathrm{C^2m^2J^{-1}}$).

For CS_2, the vibrational polarizability is [24–26]

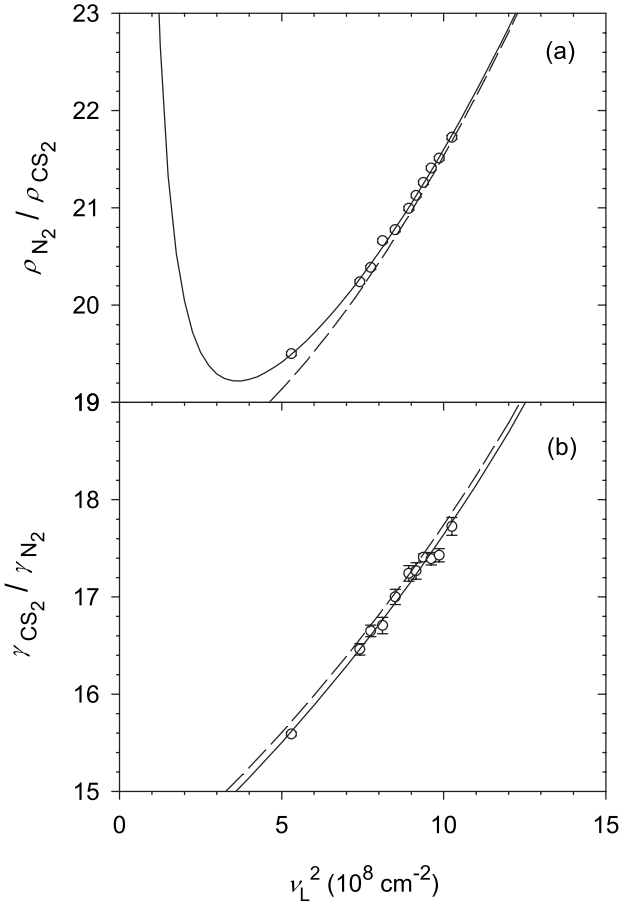

Fig. 2. (a) Phase-match density ratio and (b) hyperpolarizability ratio measurements for CS_2 and N_2 plotted versus ν_L^2. The solid curves are fit to the data (open circles), and the dashed curves show the results without the CS_2 vibrational contribution.

$$\alpha^v_{CS_2} = (3hc)^{-1} \sum_v [|\mu^z_{gv}|^2 + 2|\mu^x_{gv}|^2] \frac{2\nu_{gv}}{(\nu^2_{gv} - \nu^2)}, \tag{6}$$

and for optical frequencies $\nu >> \nu_{gv}$ this gives

$$\Delta\alpha^v_{CS_2} = (2hc)^{-1}\nu^{-2} \sum_v [|\mu^z_{gv}|^2 + 2|\mu^x_{gv}|^2]\nu_{gv}. \tag{7}$$

Infrared absorption data gives $\nu_2 = 397\ \mathrm{cm}^{-1}$ and $\mu^x_2 = 0.167 \times 10^{-30}$ Cm for the fundamental bending vibration, and $\nu_3 = 1535\ \mathrm{cm}^{-1}$ and $\mu^z_3 = 1.26 \times 10^{-30}$ Cm for the asymmetric stretching vibration [26]. Evaluating Eq. (7) with this data gives

$$\Delta\alpha^v_{CS_2} = c_4\nu^{-2}, \tag{8}$$

where $c_4 = 3.75 \times 10^6$ au cm^{-2}.

The electronic contribution $\Delta\alpha^e_{CS_2}$ for CS_2 is given by Eq. (5), with the coefficients $c_{1,CS_2} = 3.395 \times 10^{-8}\ \mathrm{au\,cm}^2$, $c_{2,CS_2} = 6.66 \times 10^{-10}\ \mathrm{cm}^2$, and $c_{3,CS_2} = 560 \times 10^{-20}\ \mathrm{cm}^4$ determined by fitting

$$\Delta\alpha_{CS_2}/\Delta\alpha_{N_2} = (\Delta\alpha^e_{CS_2} + \Delta\alpha^v_{CS_2})/\Delta\alpha_{N_2} \tag{9}$$

to the data for $\rho_{N_2}/\rho_{CS_2} = \Delta\alpha_{CS_2}/\Delta\alpha_{N_2}$.

Table 2. Calculated Hartree–Fock Electronic Hyperpolarizability for CS_2 in Atomic Units from Fig. 1 in Ref. [10]

ν (cm^{-1})	KERR	DFWM	ESHG	THG
0	11373	11373	11373	11373
5156	11563	11875	11875	12813
9400	12188	12813	13679	16875
12500	12813	14063	15938	24375
15625	13594	16250	20313	–
18750	14688	19375	27813	–

The frequency dependence of $\Delta\alpha_{CS_2}/\Delta\alpha_{N_2}$ is dominated by the dispersion of α for CS_2. The upturn at low frequencies is entirely due to the vibrational contribution from CS_2 since there is no vibrational contribution to α for N_2. The behavior seen in Fig. 2(a) is similar to that previously observed for CO_2 [24]. The value of $\Delta\alpha^v$ is nearly the same for CO_2 and CS_2, and in both cases the main contribution to $\Delta\alpha^v$ is from the asymmetric stretching vibration ν_3.

Figure 2(b) shows the ESHG data for $\gamma_{CS_2}/\gamma_{N_2}$ plotted versus ν_L^2. The fitted curves shown in Fig. 2(b) are obtained with input from the *ab initio* theoretical calculations for CS_2 to determine the electronic and vibrational contributions to γ, as is explained in what follows.

Table 2 gives the results of time-dependent Hartree–Fock (TDHF) calculations of the electronic contribution to γ_{CS_2} for four nonlinear optical (NLO) processes [10]. The basis set used for the TDHF calculations is augmented with diffuse p and d functions and 3d polarization functions. The NLO processes are distinguished by the frequency arguments in $\gamma(-\nu_\sigma; \nu_1, \nu_2, \nu_3)$, where $\gamma(-\nu; \nu, 0, 0)$ is the DC Kerr effect (KERR), $\gamma(-\nu; \nu, -\nu, \nu)$ is degenerate four-wave mixing (DFWM), $\gamma(-2\nu; \nu, \nu, 0)$ is ESHG, and $\gamma(-3\nu; \nu, \nu, \nu)$ is third-harmonic generation (THG).

Figure 3 shows the TDHF theoretical results from Table 2 plotted versus ν_L^2, where $\nu_L^2 = 2\nu^2, 4\nu^2, 6\nu^2, 12\nu^2$ for KERR, DFWM, ESHG, and THG, respectively. All the TDHF results are seen to fall on a single curve, as is theoretically predicted [22,23]. The curve fit to the TDHF results in Fig. 3 has the form

$$\gamma^e = \gamma_0^e(1 + A\nu_L^2 + B\nu_L^4 + C\nu_L^6 + D\nu_L^8), \qquad \textbf{(10)}$$

where $\gamma_0^e = \gamma_{0,HF} = 11377$ au, $A = A_{HF} = 3.531 \times 10^{-10}$ cm^2, $B = B_{HF} = 5.22 \times 10^{-20}$ cm^4, $C = C_{HF} = 2.68 \times 10^{-31}$ cm^6, and $D = D_{HF} = 1.071 \times 10^{-38}$ cm^8.

The effect of electron correlation on the calculated value for the static hyperpolarizability has been investigated by Ohta *et al.* [10], with the best estimate $\gamma_0^e = 14700$ au from a coupled cluster CCSD(T) calculation. Other results of electron-correlated calculations for CS_2 are $\gamma_0^e = 12010$ au from a CCSD calculation by Li *et al.* [12], and $\gamma_0^e = 12258$ au from a Moller–Plesset perturbation MP2 calculation by Champagne [11]. These results are also plotted in Fig. 3, and indicate that the TDHF dispersion curve underestimates γ^e by 600–2400 au.

The molecular hyperpolarizability is a function of the positions of the nuclei in the molecule. The combined vibrational contribution due to the pure vibrational response to the applied fields and zero-point vibrational averaging (ZPVA) is $\gamma^v + \Delta\gamma^{ZPVA}$ [27]. The $\Delta\gamma^{ZPVA}$ contribution is an additive correction to the electronic hyperpolarizability at the equilibrium geometry, and is included in the experimental electronic hyperpolarizability since it has similar frequency dependence. For static fields, an alternative partition of the vibrational contribution is $\gamma^{nr} + \gamma^{curv}$, the summed effect of the relaxation of the nuclear geometry and the change in curvature of the potential surface in the presence of the applied fields [27].

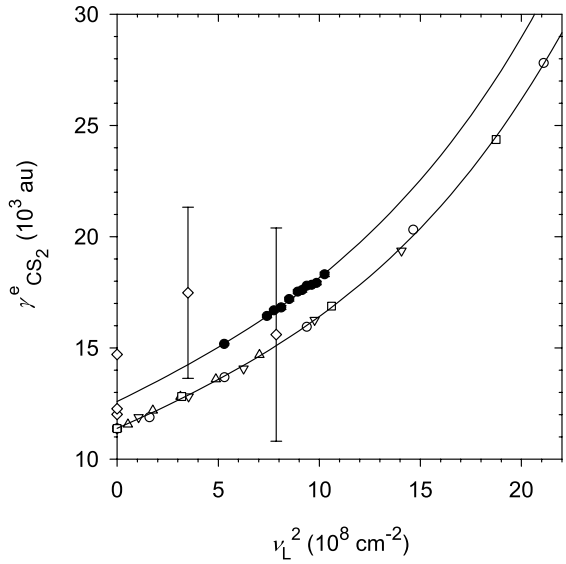

Fig. 3. Experimental and theoretical electronic hyperpolarizability results for CS_2 are plotted versus ν_L^2. The lower curve is Eq. (10) fit to the theoretical results in Table 2 for KERR (up triangles), DFWM (down triangles), ESHG (circles), and THG (squares). The upper curve is a scaled Eq. (10) fit to the experimental ESHG results (filled circles). Also shown (diamonds) are the electron-correlated static *ab initio* results from Refs. [10–12], and the experimental FWM results from Refs. [13,14].

The sum-over-states expression for γ^v can be expressed in terms of lower-order electronic response tensors $\gamma^v = [\alpha^2] + [\mu\beta] + [\mu^2\alpha] + [\mu^4]$, where the square-bracket terms are defined in Refs. [27,28], and can be evaluated by a perturbation expansion in orders of electrical and mechanical anharmonicity. For the expansion up to first-order anharmonicity, and in the static limit, $\gamma_0^v = \gamma^{nr}$ [27]. The square-bracket contributions to γ^{nr} for CS_2 have been obtained using a static finite field MP2 calculation by Champagne [11]. The results of this static calculation are $[\alpha^2]_0^{0,0} = 2578$ au, $[\mu\beta]_0^{0,0} = -398$ au, and $[\mu^2\alpha]_0^{0,1+1,0} = 1067$ au, where the superscripts indicate the order of anharmonicity. The results of this calculation give $\gamma_0^v = \gamma^{nr} = 3247$ au in the static limit.

The result for γ^v at optical frequencies, using the infinite-frequency approximation, can be expressed in terms of the static square-bracket terms [27,29]. Using the square-bracket terms from the static finite-field calculation [11], the results for CS_2 are $\gamma^v = (1/3)[\alpha^2]_0^{0,0} + (1/2)[\mu\beta]_0^{0,0} + (1/6)[\mu^2\alpha]_0^{0,1+1,0} = 838$ au for KERR, $\gamma^v = (2/3)[\alpha^2]_0^{0,0} = 1719$ au for DFWM, $\gamma^v = (1/4)[\mu\beta]_0^{0,0} = -99$ au for ESHG, and $\gamma^v = 0$ for THG.

Figure 3 shows the experimental ESHG results for γ^e obtained by subtracting $\gamma^v = -99$ au for ESHG from the

experimental results given in Table 1 for γ_{CS_2}. The experimental ESHG results for γ^e lie above and nearly parallel to the TDHF curve, and are fit with a curve which is the scaled version of Eq. (10) fit to the TDHF results, with just the leading factor $\gamma_{0,HF}$ replaced by $\gamma_0^e = \gamma_{0,ESHG} = 12592 \pm 15$ au. The scaled curve is a good fit to the data, and is consistent with the static electron-correlated *ab initio* results. The curve shown in Fig. 2(b) is obtained from the scaled TDHF curve for $\gamma^e_{CS_2}$ [Eq. (10) with $\gamma_0^e = 12592$ au] by adding $\gamma^v = -99$ au and dividing by Eq. (3) for γ_{N_2}.

The wavelength range of the data in Fig. 3 is wide enough to accurately determine the slope, but not the curvature of the γ^e experimental dispersion curve. The fit of Eq. (10) to the experimental data with both γ_0^e and A as adjustable parameters, but using the TDHF fit coefficients for B, C, D to determine the curvature, gives $\gamma_0^e = 12558 \pm 93$ au and $A = (3.58 \pm 0.12) \times 10^{-10}\,\mathrm{cm}^2$. The coefficient A determined by this fit to the experimental data is insignificantly different from the TDHF value. The result $\gamma_0^e = 12558 \pm 93$ au$(= \pm 0.7\%)$ from this fit is the best experimental estimate of γ_0^e, and this fit also gives γ^e with $\pm 0.3\%$ uncertainty for ν_L^2 in the range of the experimental data. A poor fit is obtained by translating instead of scaling the *ab initio* TDHF curve (additive instead of multiplicative correction to γ^e). This is because the larger slope of the scaled TDHF curve matches the slope of the experimental data, whereas the unchanged slope for the translated curve is too small.

The result for $\gamma^e_{CS_2}$ from a recent gas-phase experiment by Reichert *et al*. [13,14] is also shown in Fig. 3. This beam-deflection experiment measures $\gamma(-\nu_2; \nu_1, -\nu_1, \nu_2)$, where ν_1 is the pump laser frequency and ν_2 is the probe frequency, and is calibrated using the previously measured CS_2 polarizability anisotropy. For this NLO process, γ^v is given by $\gamma^v = [\alpha^2]_0^{0,0} f(\nu_1, \nu_2)$, where [30]

$$f = \frac{1}{3}\left[1 + \left[1 - \frac{(\nu_1 - \nu_2)^2}{\nu_{01}^2}\right]^{-1} + \left[1 - \frac{(\nu_1 + \nu_2)^2}{\nu_{01}^2}\right]^{-1}\right], \tag{11}$$

and $\nu_{01} = 658\,\mathrm{cm}^{-1}$ is the frequency for the Raman-active fundamental symmetric stretching vibration in CS_2. For this experiment, with 1250 nm pump and 950 nm probe wavelength, $f = 0.309$ and $\gamma^v = 796$ au. Subtracting γ^v from $\gamma_{CS_2} = (18.3 \pm 3.9) \times 10^3$ au reported in Ref. [13] ($\times 6$ to change to the Taylor series convention [31,32]) gives $\gamma^e_{CS_2} = (17.5 \pm 3.9) \times 10^3$ au at $\nu_L^2 = 3.5 \times 10^8\,\mathrm{cm}^{-2}$. This result is plotted in Fig. 3, and it agrees with the results of the present experiment.

The DC Kerr result $\gamma = (114 \pm 10) \times 10^3$ au at $\lambda = 632.8$ nm ($\nu_L^2 = 5.0 \times 10^8\,\mathrm{cm}^{-2}$) from Bogaard *et al*. [7] is the only other gas-phase measurement for CS_2, and it disagrees with all other measurements and calculations. The early liquid phase ESHG result $\gamma = (38 \pm 6) \times 10^3$ au at $\lambda = 1064$ nm ($\nu_L^2 = 5.3 \times 10^8\,\mathrm{cm}^{-2}$) from Levine *et al*. [8] also disagrees with the present results. These Kerr and ESHG results are off-scale on Fig. 3. The disagreement for the ESHG result cannot be attributed to the liquid state, since recent experiments [2,3,13,14] using the beam deflection technique (with 800 nm pump and 650 nm probe) find $\gamma = (16.4 \pm 4.8) \times 10^3$ au at $\nu_L^2 = 7.9 \times 10^8\,\mathrm{cm}^{-2}$ for liquid CS_2, in good agreement with the present gas-phase results. Figure 3 shows γ^e obtained by subtracting $\gamma^v = 812$ au for this point.

4. CONCLUSION

The frequency-dependent electronic hyperpolarizability γ^e for CS_2 has been determined using the combined results of the present experiment and previous *ab initio* calculations, with uncertainty 0.3% for γ^e over the frequency range of the experimental measurements and estimated uncertainty 0.7% for γ^e at the static limit. All NLO processes are represented by a single dispersion curve for γ^e versus ν_L^2. The TDHF calculation for γ^e appears to accurately determine the shape of the dispersion curve, but *ab initio* static values for γ^e obtained with HF, MP2, CCSD, and CCSD(T) methods and an augmented basis set differ by up to 20% from the experimental result and from each other. The observed hyperpolarizability γ is the sum of γ^e and the vibrational hyperpolarizability γ^v, where the calculated value of γ^v for the considered NLO processes is $<10\%$ of the total γ at optical frequencies for CS_2.

Disclosures. The authors declare no conflicts of interest.

REFERENCES

1. R. W. Boyd, *Nonlinear Optics*, 3rd ed. (Academic, 2008).
2. M. Reichert, H. Hu, M. R. Ferdinandus, M. Seidel, P. Zhao, T. R. Ensley, D. Peceli, J. M. Reed, D. A. Fishman, S. Webster, D. J. Hagan, and E. W. VanStryland, "Temporal, spectral, and polarization dependence of the nonlinear optical response of carbon disulfide," Optica **1**, 436–445 (2014).
3. M. Reichert, H. Hu, M. R. Ferdinandus, M. Seidel, P. Zhao, T. R. Ensley, D. Peceli, J. M. Reed, D. A. Fishman, S. Webster, D. J. Hagan, and E. W. VanStryland, "Temporal, spectral, and polarization dependence of the nonlinear optical response of carbon disulfide: erratum," Optica **3**, 657–658 (2016).
4. X.-Q. Yan, X.-L. Zhang, S. Shi, Z.-B. Liu, and J.-G. Tian, "Third-order nonlinear susceptibility tensor elements of CS_2 at femtosecond time scale," Opt. Express **19**, 5559–5564 (2011).
5. G. Boudebs and K. Fedus, "Absolute measurement of the nonlinear refractive indices of reference materials," J. Appl. Phys. **105**, 103106 (2009).
6. P. Zhao, M. Reichert, S. Benis, D. J. Hagan, and E. W. VanStryland, "Temporal and polarization dependence of the nonlinear optical response of solvents," Optica **5**, 583–594 (2018).
7. M. P. Bogaard, A. D. Buckingham, and G. L. D. Ritchie, "The temperature-dependence of electric birefringence in gaseous benzene and carbon disulfide," Mol. Phys. **18**, 575–576 (1970).
8. B. F. Levine and C. G. Bethea, "Second and third order hyperpolarizabilities of organic molecules," J. Chem. Phys. **63**, 2666–2682 (1975).
9. G. Maroulis, "Electric moments, polarizabilities and hyperpolarizabilities for carbon disulfide (S = C = S) from accurate scf calculations," Chem. Phys. Lett. **199**, 250–256 (1992).
10. K. Ohta, T. Sakaguchi, K. Kamada, and T. Fukumi, "Ab initio molecular orbital calculations of the second hyperpolarizability of the carbon disulfide molecule: electron correlation and frequency dispersion," Chem. Phys. Lett. **274**, 306–314 (1997).
11. B. Champagne, "Ab initio determination of the nuclear relaxation contribution to the second hyperpolarizability of carbon disulfide," Chem. Phys. Lett. **287**, 185–188 (1998).
12. W. Li, W. Q. Tian, and X. Sun, "Understanding of nonlinear optical properties of CS_2 from a microscopic viewpoint," J. Chem. Phys. **137**, 084315 (2012).

13. M. Reichert, P. Zhao, J. M. Reed, T. R. Ensley, D. J. Hagan, and E. W. VanStryland, "Beam deflection measurement of bound-electronic and rotational nonlinear refraction in molecular gases," Opt. Express **23**, 22224–22237 (2015).
14. M. Reichert, P. Zhao, J. M. Reed, T. R. Ensley, D. J. Hagan, and E. W. VanStryland, "Beam deflection measurement of bound-electronic and rotational nonlinear refraction in molecular gases: erratum," Opt. Express **24**, 19122 (2016).
15. D. P. Shelton and A. D. Buckingham, "Optical second-harmonic generation in gases with a low-power laser," Phys. Rev. A **26**, 2787–2798 (1982).
16. V. Mizrahi and D. P. Shelton, "Dispersion of nonlinear susceptibilities of Ar, N_2, and O_2 measured and compared," Phys. Rev. Lett. **55**, 696–699 (1985).
17. D. P. Shelton, "Nonlinear optical susceptibilities of gases measured at 1064 and 1319 nm," Phys. Rev. A **42**, 2578–2592 (1990).
18. E. A. Donley and D. P. Shelton, "Hyperpolarizabilities measured for interacting molecular pairs," Chem. Phys. Lett **215**, 156–162 (1993).
19. D. P. Shelton and V. Mizrahi, "Refractive-index dispersion of gases measured by optical harmonic phase matching," Phys. Rev. A **33**, 72–76 (1986).
20. J. H. Dymond and E. B. Smith, *The Virial Coefficients of Pure Gases and Mixtures* (Oxford, 1980).
21. Landolt-Bornstein, *Zahlenwerte und Funktionen, Band II, Teil 8* (Springer, 1962).
22. D. P. Shelton and J. E. Rice, "Measurements and calculations of the hyperpolarizabilities of atoms and small molecules in the gas phase," Chem. Rev. **94**, 3–29 (1994).
23. D. M. Bishop and D. W. DeKee, "The frequency dependence of nonlinear optical processes," J. Chem. Phys. **104**, 9876–9887 (1996).
24. D. P. Shelton, "Hyperpolarizability dispersion measured for CO_2," J. Chem. Phys. **85**, 4234–4239 (1986).
25. M. Guerreiro, N. Bras, M. Blain, and J.-M. Leclercq, "Ab initio calculations of the vibrational contributions to the static dipole polarizability of CO_2 and CS_2," Chem. Phys. Lett. **274**, 315–322 (1997).
26. D. M. Bishop and L. W. Cheung, "Vibrational contributions to molecular polarizabilities," J. Phys. Chem. Ref. Data **11**, 119–133 (1982).
27. D. M. Bishop, "Molecular vibration and nonlinear optics," Adv. Chem. Phys. **104**, 1–40 (1998).
28. D. M. Bishop, J. M. Luis, and D. Kirtman, "Additional compact formulas for vibrational dynamic polarizabilities and hyperpolarizabilities," J. Chem. Phys. **108**, 10013–10017 (1998).
29. D. M. Bishop and E. K. Dalskov, "Analysis of the vibrational, static and dynamic, second hyperpolarizability of five small molecules," J. Chem. Phys. **104**, 1004–1011 (1996).
30. D. P. Shelton, "Vibrational contributions to the hyperpolarizabilities of homonuclear diatomic molecules," Mol. Phys. **60**, 65–76 (1987).
31. A. Willetts, J. E. Rice, D. M. Burland, and D. P. Shelton, "Problems in the comparison of theoretical and experimental hyperpolarizabilities," J. Chem. Phys. **97**, 7590–7599 (1992).
32. H. Reis, "Problems in the comparison of theoretical and experimental hyperpolarizabilities revisited," J. Chem. Phys. **125**, 014506 (2006).